THE ASTROPHYSICAL JOURNAL, 377:480–491, 1991 August 20

PHOTOIONIZATION MODELING OF MAGELLANIC CLOUD PLANETARY NEBULAE. II.[1]

M. A. DOPITA AND S. J. MEATHERINGHAM
Mount Stromlo and Siding Spring Observatories, Institute of Advanced Studies, The Australian National University, Private Bag, Weston Creek P.O., ACT 2611, Australia
Received 1990 September 27; accepted 1991 February 25

ABSTRACT

We present the results of self-consistent photoionization modeling of a further sample of 44 Magellanic Cloud Planetary Nebulae (PN), to derive a Hertzsprung-Russell (H-R) diagram for the central stars, chemical abundances and the nebular parameters.

We find that, for optically thick PN, the transformation between the "observed" Hertzsprung-Russell (H-R) diagram; the log (Hβ): excitation class plane, and the "true" H-R diagram: the log $(L/L_\odot)$:log $(T_{\rm eff})$ plane, is particularly simple. We also find a very tight relation between the reduced mass of the nebula, that is, the ionized mass corrected to unit luminosity of the central star, and the nebular radius.

From their positions on the H-R diagram, we conclude that the majority of the central stars in this sample have masses between 0.55 and 0.7 $M_\odot$, but that the type I PN have generally higher mass central stars, ranging up to 1.2 $M_\odot$. These objects are observed mostly during the fading part of their evolution, consistent with their expected more rapid evolution across the H-R diagram.

We find that there is clear evidence for a spread in the abundances of the alpha-process elements in both Clouds which is probably a consequence of the spread in ages of the PN precursor stars. For the LMC there is also a correlation between core mass and metallicity for these elements. In the future, this relationship may allow us to derive age: metallicity relationships for the Clouds.

For the type I PN we find that, not only do they lie on a distinct sequence on the N/O versus He/H diagram, but also, they appear to be deficient in O, with respect to the other alpha-process elements. We interpret this as evidence for not only for CN processing, dredge-up and ejection, but also for appreciable NO processing having taken place.

Subject headings: galaxies: Magellanic Clouds — nebulae: abundances — nebulae: planetary — stars: early-type

1. INTRODUCTION

The Magellanic Cloud sample has been the subject of a systematic and detailed study by us and our group in recent years, and data on the diameters, fluxes, expansion velocities and kinematics has been accumulated (Dopita et al. 1985, 1987, 1988; Dopita, Ford, & Webster 1985; Meatheringham et al. 1988; Meatheringham, Dopita, & Morgan 1988; Wood, Bessell, & Dopita 1986; Wood et al. 1987). This has led to a general understanding of the outlines of the evolutionary sequence (Dopita & Meatheringham 1990).

However, a detailed understanding of the variety of evolutionary behavior, and mass dependence of the pre-planetary nebular mass-loss and chemical dredge-up processes can only be obtained from the detailed modeling and spectrophotometric analysis of individual PN. In two earlier papers (Meatheringham & Dopita 1991a, b) we have presented new high-quality spectrophotometry for a total of 77 different PN in the Magellanic Clouds. Detailed photoionization models have been constructed for the first group of these (Dopita & Meatheringham 1991, hereafter Paper I). In this paper we present models based on the spectrophotometric results presented by Meatheringham & Dopita (1991b). This database has the advantage of a good wavelength coverage (~3400–8000 Å), a good sensitivity and dynamic range (greater than 300), and a spectral resolution of ~5 Å, which is more than adequate to resolve important diagnostic lines such as the [S II] 6717, 31 Å doublet, the [O III] 4363 Å line from Hγ, or the various lines in the range 4686–4740 Å.

The objects observed are all drawn from the Sanduleak, MacConnell, & Philip (1978) list, which is a fairly uniform magnitude limited sample. While the group modeled in Paper I was chosen to cover the full range of excitation classes and densities exhibited by the brighter Magellanic Clouds PN, the current sample includes many more of the faintest SMP objects. However, the faintest objects identified as PN in the Clouds such as the Jacoby PN studied by Henry, Leibert, & Boronson (1989), are still not well-represented in this sample. Nonetheless, as we will show below, by combining the results of both papers we may draw important conclusions about the evolution of PN and about the chemical evolution in both of the Magellanic Clouds.

2. PHOTOIONIZATION MODELING

2.1. *Photoionization Modeling*

In Paper I, we described in detail our photoionization modeling procedure. We have used the same procedure here, and we refer the reader to Paper I for details.

Briefly, in order to determine the PN nebular abundances, and to place the central star on the HR diagram we require to know only the absolute Hβ flux, the nebular density, and to have accurate spectrophotometry over as wide a wavelength as

[1] The authors would like to dedicate this paper to the memory of Dr. Betty Louise Webster, who died on 1990 September 29 after a long and heroic struggle with cancer. We will remember her as a gentle but inspiring friend and collaborator. Her doctoral thesis, obtained from the ANU in 1966, blazed the trail in the study of the planetary nebulae in the Magellanic Clouds, and this paper owes a lot to her inspiration and continuing interest.

possible. This is possible because, with the aid of a photoionization code, the ionization temperature can be determined from the nebular excitation, the luminosity of the central star can be determined from the absolute Hβ flux, and the chemical abundances can be determined from the electron temperature of the nebula and from the details of its emission line spectrum. We have used the generalized modeling code MAPPINGS (Binette, Dopita, & Tuohy 1985) to compute the emission line spectra of isobaric model PN in photoionization equilibrium with a central star having a blackbody distribution in frequency. Models having central stars with effective temperatures lower than about 90,000 K have the ionizing spectrum cut off above 4 Ryd.

The nebular gas was assumed to have a filling factor of unity in the emitting volume, but to have a shell structure with a sharp inner radius defined by the interface between the swept-up material lost from the star during the AGB and the hot, shocked, stellar wind of the PNn. The outer boundary is set either by the Strömgren sphere of the central star in the case of optically thick models, or by truncation of the model at a finite optical depth at the Lyman Limit, in the case of optically thin nebulae. The pressure invariant of the models is computed in terms of the pressure that would be produced by a hydrogen plasma of a given density at a temperature of 10^4 K, Thus, with appropriate temperature correction, this nominal density can be thought of as the density of the model as derived either from the observed [S II] 6717/6731 Å line ratio, or from the [O II] 3727/3729 Å line ratio (Meatheringham & Dopita 1991a, b; Dopita et al. 1988; Barlow 1987; Monk, Barlow, & Clegg 1988).

The absolute Hβ flux is derived from the fluxes given by Meatheringham, Dopita, & Morgan (1988), supplemented with data given in Wood, Bessell, & Dopita (1986) and Wood et al. (1987). A true distance modulus of $(m - M)_0 = 18.5$ is assumed for the LMC, and a modulus of $(m - M)_0 = 18.8$ is taken for the SMC (Feast & Walker 1987). The reddening constant derived from the spectrophotometry of each object is then used in the derivation of the absolute Hβ luminosity.

2.2. *Determination of Stellar Parameters*

The photon energy distribution determines the excitation class (E.C.), which measures the degree of ionization of helium with respect to hydrogen. We will use here the classification given by Dopita & Meatheringham (1990), which, since it was defined in terms of two diagnostic line ratios, is a continuous variable. For objects in the range $0 < \text{E.C.} < 5$ it is determined primarily from the [O III] to Hβ ratio, while for objects in the range $5 < \text{E.C.} < 10$ it is determined by the He II/Hβ ratio. A very useful secondary indicator is the [Ne III] to Hβ ratio, and, provided that the density is well-known, we may also use the ratio of the [O I], [O II] and [O III] lines. Taken together, these ratios are sufficient to fix the excitation temperature of the ionizing radiation with a model-dependent error about ± 0.04 dex.

Given the effective temperature, the luminosity of the central star is determined by the absolute Hβ flux, in the case of optically thick objects. The luminosity was adjusted until the observed and the model line fluxes agreed. Given that the intrinsic error in the observed fluxes is about ± 0.03 dex, the error in the distance modulus is ± 0.15 dex, and the error in the reddening constant is 0.04, we estimate that derived luminosities would have a typical random error of ± 0.07 dex and a systematic error of ± 0.15 dex.

In the case of optically thin objects it is still possible to make a reasonably accurate estimate of the luminosity. This is possible because the onset of optical thinness produces an unequivocal spectral signature. Nebulae with increasing degrees of optical thinness show first a weakening and then a disappearance of the [O I] and [N I] lines, followed by a weakening of the singly ionized He, O, and N species accompanied by an increase in the [O III]/Hβ and [Ne III]/Hβ line ratios. Finally, for very optically thin models, the [O III]/Hβ line ratio decreases, and the He II 4686 Å line, if initially present, increases in its relative line intensity. It is difficult to quantify the modeling errors in the determination of stellar luminosity in the case of optically thin nebulae. However, it is clear that the errors increase as the optical depth in the nebula decreases. The additional error involved when the optical depth is as low as unity is of order ± 0.1 dex in the luminosity. However, the additional error involved in the temperature estimate is smaller, about ± 0.03 dex.

2.3. *The Derivation of Abundances*

For a given stellar temperature, the abundances determine the electron temperature, and hence the [O III] 4363/5007 Å line ratio. In order to have a reasonable first guess for the nebular abundances, the abundance set obtained by Russell & Dopita (1990) was initially assumed. These abundances were also derived using MAPPINGS, but applied to observations of H II regions and SNR in the Magellanic Clouds. The C/O ratio is high for PN in both our Galaxy and in the case of the small number of non-type I objects so far studied in the ultraviolet with *IUE* (Aller et al. 1987). For type I objects in the Magellanic Clouds the C/O ratio observed with IUE is low (Aller et al. 1987; Meatheringham et al. 1990), reflecting the differences in burning and dredge-up processes expected to occur in these objects (Renzini & Voli 1981). For the purposes of modeling, we assumed that non-type I objects (with $\text{N/O} < 0.3$) have a typical C/O ratio of 1.5, and that type I objects have C/O of 0.1. However, errors in the assumed value have only a second-order impact on the derived abundances. The most serious modeling errors for the type I objects appear to result from the fact that the models cannot reproduce the high electron temperatures observed in the [O III] zone, and that they fail to reproduce the intensities of the highest excitation lines, such as [Ne V]. Certainly, the low value of the assumed C/O ratio goes some way towards redressing the balance, but it would appear that an additional heating mechanism is required in the inner portion of the nebula. We may speculate that the cause of this heating is mechanical, the result of the strong stellar winds in type I objects, analogous to the additional heating needed to explain the excitation conditions in the faint outer halos of some PN (Middlemass et al. 1991).

The overall nebular abundances, the luminosity, and the temperature of the central star were iterated as described above until the nebular flux, excitation, and temperatures agreed, within the errors, with the photoionization models. The pressure parameter is determined by forcing agreement between the predicted and observed [S II] and [O II] densities. When the parameters of the photoionization model all agree, within the errors of observation and modeling, with the observed parameters of the PN, the abundances of N, S, Ne, and Ar are fine tuned to give the best agreement with observation. This point is typically reached after five iterations.

3. RESULTS

3.1. *Parameters of the Central Stars*

The effective temperatures and luminosities of the central stars, as derived from the modeling of the objects for which spectrophotometry was presented by Meatheringham & Dopita (1991b), are given in Table 1. This list, when combined with the results of Paper I, more than quadruples the number of Magellanic Cloud PNn which have been placed on the Hertzsprung-Russell Diagram (see Aller et al. 1987; Monk et al. 1988).

The excitation class turns out to give an excellent measure of the excitation balance temperature (see Fig. 1). The correlation between excitation class, E, and $\log(T_{\rm eff})$ is excellent. A least-squares fit gives

$$\log(T_{\rm eff}) = (4.489 \pm 0.017) + (0.1124 \pm 0.0025)E - (0.00172 \pm 0.00037)E^2 , \quad (3.1)$$

with a correlation coefficient of 0.98. The errors are the formal errors of the fit.

For the optically thick objects, there also exists a tight correlation between the luminosity of the central star with the luminosity in Hβ and the excitation class (Fig. 2). This is to be expected, since, in an optically thick nebula, Strömgren theory shows that the number of recombinations is primarily dependent upon the number of ionizing photons produced by the

TABLE 1

PARAMETERS OF THE PLANETARY NEBULAE AS DETERMINED FROM THE NEBULAR MODELS

Object	L_* ($L_\odot$)	$T_{\rm eff}$ (K)	$P/10^4$ (cm^{-3} K)	$R_{\rm in}$ (pc)	$R_{\rm out}$ (pc)	$M_{\rm neb}$ ($M_\odot$)	$\tau_{\rm out}$ (H)
			LMC				
SMP 02	810	42000	5000	0.005	0.036	0.037	
SMP 03	1000	47000	6800	0.010	0.032	0.025	3.01
SMP 06	6130	140000	17000	0.049	0.057	0.133	
SMP 07	2600	225000	2250	0.039	0.130	0.522	
SMP 13	5210	140000	9700	0.032	0.064	0.238	
SMP 14	700	265000	500	0.042	0.209	0.663	
SMP 16	1690	200000	1400	0.039	0.147	0.513	
SMP 19	4830	158000	4830	0.081	0.125	0.518	
SMP 24	525	200000	1850	0.016	0.079	0.115	
SMP 29	3300	200000	6700	0.010	0.067	0.216	
SMP 32	3000	188000	5200	0.010	0.074	0.205	
SMP 33	4060	155000	7600	0.029	0.065	0.201	
SMP 35	1485	118000	2420	0.013	0.097	0.256	
SMP 38	3280	95000	12500	0.026	0.045	0.115	
SMP 40	1100	185000	1650	0.010	0.117	0.290	
SMP 41	590	175000	2400	0.003	0.071	0.097	
SMP 42	1600	70000	15000	0.010	0.027	0.032	3.05
SMP 44	305	175000	1400	0.006	0.077	0.086	
SMP 45	1580	116000	1580	0.013	0.135	0.438	
SMP 46	335	145000	4900	0.019	0.039	0.027	
SMP 48	3700	59000	12000	0.019	0.043	0.123	
SMP 54	795	227000	1230	0.029	0.111	0.219	
SMP 55	4850	37000	34800	0.013	0.019	0.029	
SMP 60	2040	257000	1000	0.032	0.137	0.211	6.06
SMP 61	4266	61000	30000	0.052	0.053	0.047	
SMP 62	4710	127000	6000	0.032	0.088	0.437	
SMP 67	2130	44000	3200	0.013	0.065	0.156	
SMP 72	910	180000	500	0.055	0.181	0.234	3.70
SMP 73	7120	135000	4300	0.039	0.119	0.768	
SMP 74	7080	117000	7000	0.065	0.090	0.484	
SMP 76	4805	54000	13000	0.013	0.044	0.128	
SMP 78	6040	130000	5400	0.032	0.092	0.456	
SMP 85	7000	41500	46000	0.013	0.019	0.034	
SMP 87	6530	225000	2600	0.081	0.149	0.861	
SMP 92	9130	142000	13000	0.065	0.076	0.242	
SMP 99	5700	124000	3300	0.055	0.124	0.679	
SMP 101	3000	160000	6500	0.013	0.062	0.152	8.00
			SMC				
SMP 02	4780	130000	4100	0.016	0.117	0.688	
SMP 03	2420	96000	2300	0.019	0.099	0.259	3.00
SMP 05	2780	147000	4900	0.032	0.082	0.273	
SMP 06	5950	76000	31500	0.026	0.035	0.099	
SMP 11	3310	45000	1500	0.016	0.160	0.720	
SMP 14	2300	133000	4400	0.016	0.083	0.245	
SMP 28	1925	152000	2780	0.026	0.095	0.297	

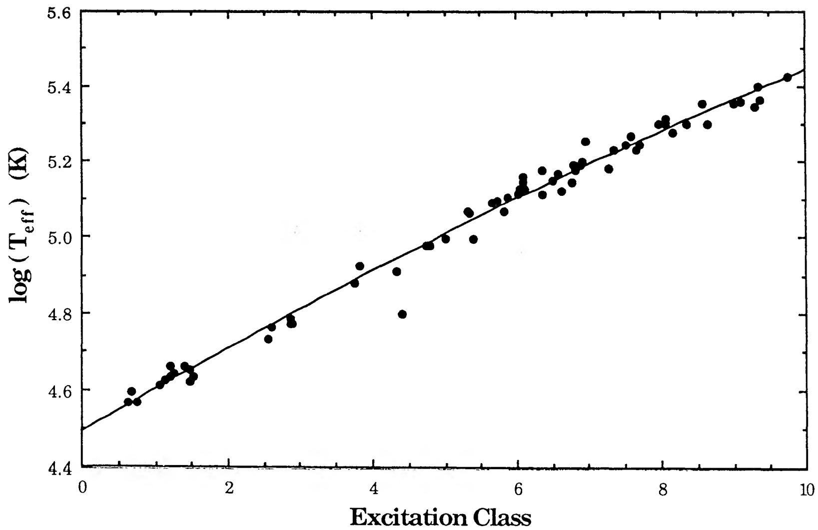

FIG. 1.—Correlation between the excitation class, and the excitation balance temperature derived from models for all the optically thick PN in the measured in the Clouds. The line is a least-squares quadratic fit.

central star, and, to only a secondary degree, upon the effective temperature of the central star. The correlation may be written

$$\begin{aligned}\log (L/L_\odot) = {} & \log (L_{\mathrm{H}\beta}/L_\odot) + (2.32 \pm 0.02) \\ & - (0.179 \pm 0.016)E + (0.035 \pm 0.004)E^2 \\ & - (0.00166 \pm 0.00035)E^3 \,. \qquad (3.2)\end{aligned}$$

Equations (3.1) and (3.2) provide a useful transformation between the parameters of the "observed" Hertzsprung-Russell (H-R) plane; $\log (L_{\mathrm{H}\beta}/L_\odot)$ and E, and the "theoretical" H-R parameters; $\log (L/L_\odot)$ and $\log (T_{\mathrm{eff}})$.

The H-R diagram resulting from our analysis is shown in Figures 3 and 4, for the LMC and the SMC, respectively, where the optically thick, optically thin, and type I PN are distinguished by separate symbols. In the region where the PNn are evolving to higher temperatures at nearly constant luminosity, the optically thick objects are found in a range of core masses between 0.54–0.68 $M_\odot$ in the LMC and 0.56–0.72 $M_\odot$ in the SMC. Optically thin PN occupy a broad region of the diagram, and may have a somewhat lower mean mass. It is very evident that the mean mass is higher, and the range of core masses wider, than those derived by Schönberner (1981) for a group of nearby, evolved PNn. Despite our efforts to select the PN to be observed throughout the range of flux, density, and excitation class, our sample still suffers from selection effects, since the faintest PN will tend to be missed. This is particularly evident in the case of the SMC, for which very few objects with $\log (L/L_\odot) < 3.3$ are observed.

Note that the type I PN are found preferentially at high T_{eff}, lower luminosities and, in general, at larger values of the core

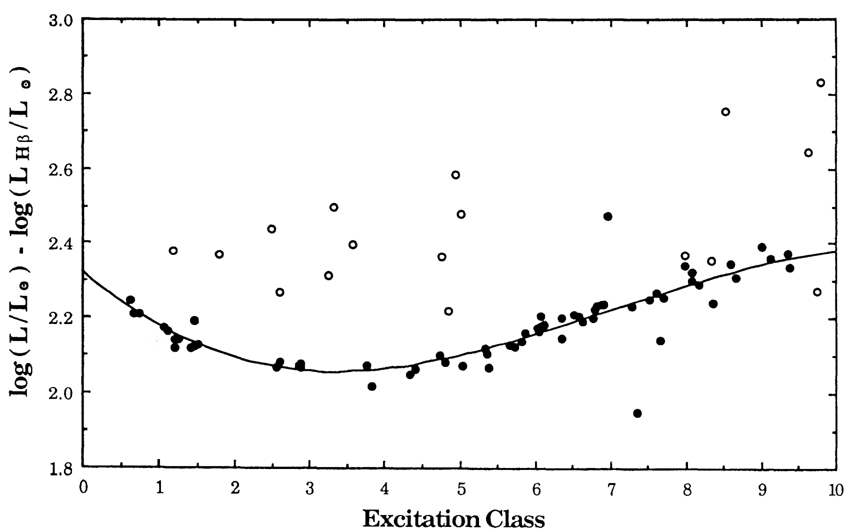

FIG. 2.—Relationship between the observed absolute Hβ flux (ergs s^{-1}), and the luminosity of the central star, plotted as a function of the excitation class. Open circles represent optically thin PN, and filled circles the optically thick objects. The curve is a least-squares cubic fit. The relationships of Figs. 1 and 2 together allow the transformation of the "observed" Hertzsprung-Russell diagram; ($\log F(\mathrm{H}\beta)$: E.C.) to the "true" H-R diagram; ($\log (L/L_\odot)$: $\log T_{\mathrm{eff}}$) for the optically thick objects.

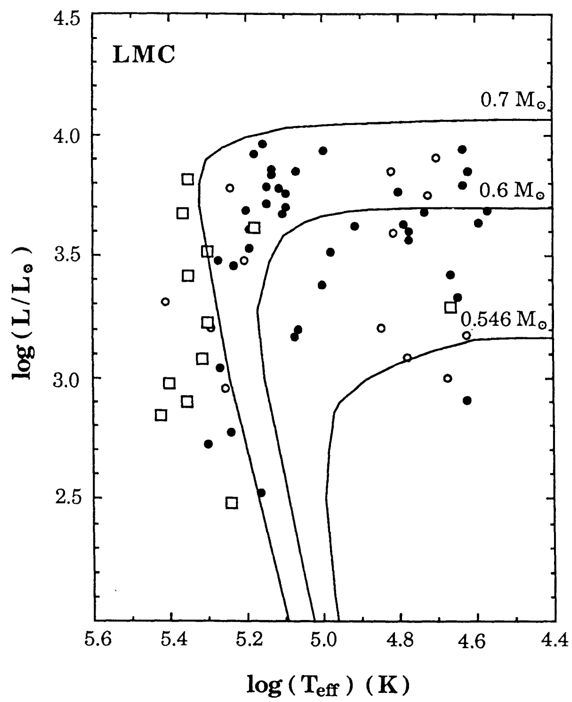

FIG. 3.—Hertzsprung-Russell diagram for the Large Magellanic Cloud PN. The evolutionary tracks for different core masses are from Schönberner (1981) and Wood & Faulkner (1986). The open circles represent optically thin objects, the filled circles optically thick PN and the open squares are type I Planetaries. The type I objects are objects of higher core mass, up to $1.3 M_\odot$.

mass. This is consistent with the type I PN representing the more massive progenitor stars, and therefore, as a result of their rapid evolution across the Diagram, are preferentially found at high effective temperatures on the descending portions of the evolutionary tracks. The objects with the most massive cores, in the range 1.0–1.3 $M_\odot$, are also among the most extreme type I objects in the sample, with N/O ratios in the range 0.7–1.63. These include LMC SMP 14, 54, 87, and 96.

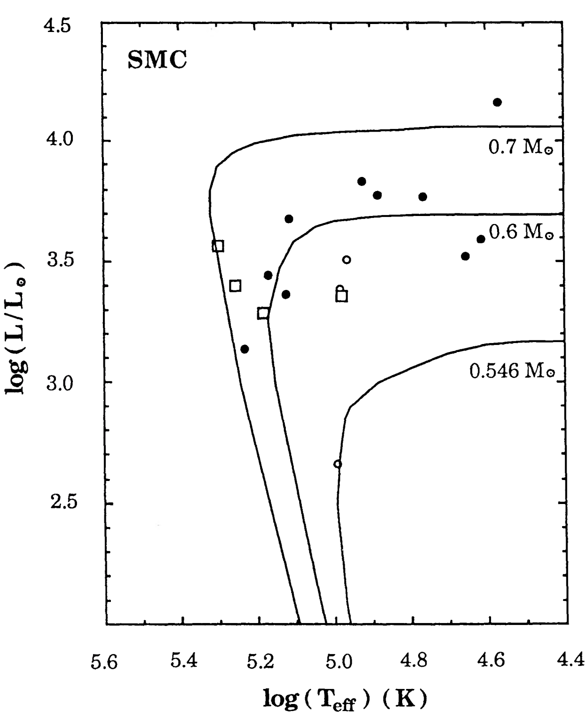

FIG. 4.—Same as Fig. 5, for the SMC PN

Although the extension of the sample to fainter PN has improved the representation of objects on the descending portions of the evolutionary tracks, it is clear that both observational selection and evolutionary effects will tend to broaden the true mass range of PNn still further (Shaw 1989). That this is indeed the case is made clear by the comparison with the evolutionary tracks which shows that these fainter objects, both of type I and of other types, have generally somewhat higher core masses, on average. In future papers we will present data on the Morgan & Good (1985) sample, and on the new Morgan (1991) sample, which will push the magnitude limit down even fainter.

3.2. *Nebular Parameters*

The derived nebular parameters are given in Table 1. The inner radius, $R_{\rm in}$, represents the boundary between the swept-up photoionized gas and the hot shocked stellar wind, and is not very well-determined. If it is made too large, the ionization parameter falls too low, and lines of low-ionization degree become too strong. The observations require an ionization parameter typically in the range $3 \times 10^8 > \langle Q \rangle > 5 \times 10^7$ cm s^{-1}, so with a given nebular pressure parameter, this determines the inner radius to an accuracy of about a factor of 2. The nebular pressure parameter P is chosen to give best agreement with the [O II] and [S II] densities. With a given luminosity, density, pressure parameter, and hydrogen optical depth, $\tau_{\rm out}$, the outer radius, $R_{\rm out}$, is then determined. Direct observational data on the outer radius is very sparse, which is regrettable, since this would have provided an useful test for consistency of the model. Speckle interferometry (Wood, Bessell, & Dopita 1986) tends to pick up on condensed central cores of nebulae rather than on the fainter outer shell (Dopita & Meatheringham 1990). Direct imaging (Wood et al. 1987) is limited to only the larger and fainter nebulae. For the rest, they will have to wait until high-resolution images have been obtained using *HST*.

The models return the mean hydrogen particle density in the nebula. The total mass of the nebula is derived from this quantity via the formula

$$M_{\rm neb} = (4/3)\pi(R_{\rm out}^3 - R_{\rm in}^3)m_{\rm H} N_{\rm H}[1 + 4Z({\rm He})] , \quad (3.3)$$

where $m_{\rm H}$ is the mass of the hydrogen atom, and Z(He) is the abundance of helium, by number with respect to hydrogen. The uncertainty in $R_{\rm in}$ has little effect on the accuracy of the result.

Gathier et al. (1983), and, more recently, Pottasch & Acker (1989) have pointed out the strong relationship between nebular mass and nebular radius. They argue, as have Dopita & Meatheringham (1990), that this relationship is strong evidence in support of the idea that the majority of these PN are optically thick. Our photoionization analysis demonstrates that many of these PN are in fact optically thick. In Figure 5 we plot the log (R):log (M) relation for all PN analyzed here and in Paper I. For the optically thick objects, there is a linear correlation with a slope of 1.6 ± 0.1. The optically thin objects scatter below and to the right of this line, as would be expected. However, we confirm the results of Paper I, that optically thin nebulae are found at all radii, even in PN of small radius having relatively unevolved central stars of low effective tem-

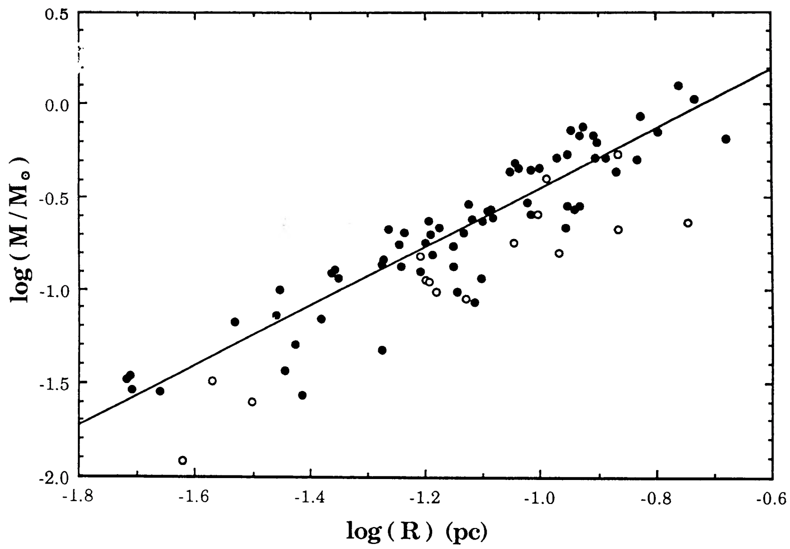

FIG. 5.—Simple nebular mass: radius relationship for the Magellanic Cloud PN. The open circles are for optically thin objects, and the filled circles apply to the optically thick objects.

perature, and also that we find no clear transition from optically thick to optically thin PN at a critical value of the radius.

In the two-wind model of PN, a fast radiation-pressure driven wind from the central star is interacting with the slow wind previously ejected while the star was on the AGB. In the PN phase, the hot shocked stellar wind from the PNn provides the pressure which confines the ionized portion of the old AGB wind to a thin shell. Dopita & Meatheringham (1990) have shown that, since the pressure of the stellar wind is in equilibrium with the gas pressure in the H II region and the extent of the H II region is determined by the ionizing flux from the central star, S_*, the following relationship exists between the thickness of the ionized shell, ΔR, of density, n, and radius, R:

$$R = \text{constant } (\Delta R/R)/(1 - \Delta R/R)^4 \; ; \qquad (3.4)$$
$$n = \text{constant } S_*^{1/2} R^{-3/2} (\Delta R/R)^{-1/2}$$

For optically thick PN, the above equations permit us to derive a reduced mass: radius relationship, where the reduced mass is the nebular mass corrected to unit luminosity of the central star. This is shown in Figure 6.

This gives an excellent description for the optically thick sequence, and removes much of the intrinsic scatter seen in Figure 5. The least-squares slope is 1.67 ± 0.05, with a correlation coefficient of 0.94. We also show on Figure 5 the slope resulting from equations (3.4), normalized at $\log (R) = -1.1$ pc. The fact that the observational slope agrees so well with this theoretical line is an indication that the simple two-wind model is valid, at least to first-order. Again, optically thin objects are found below and to the right of the correlation, with no clear transition from an optically thick to optically thin sequence. Thus the intrinsic scatter in the wind parameters during the AGB phase of evolution must be quite large.

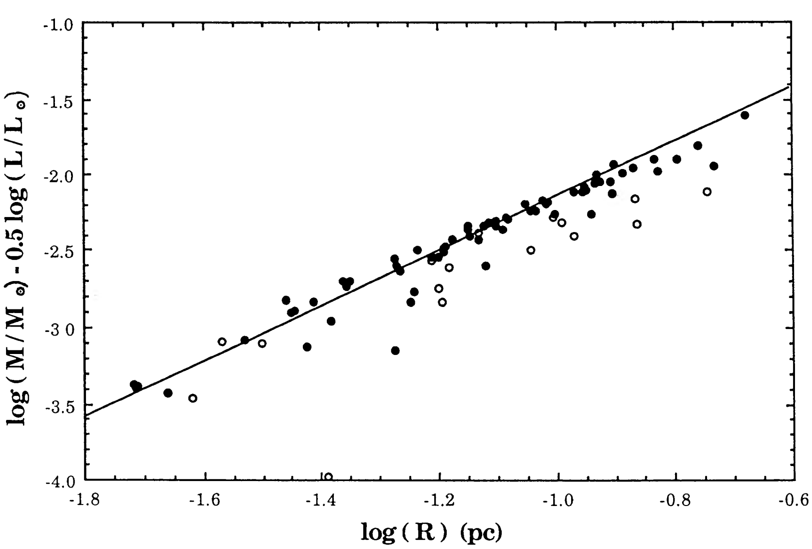

FIG. 6.—" Reduced," i.e., luminosity-corrected, nebular mass: radius relation for the Magellanic Cloud PN. The open circles are for optically thin objects, and the filled circles apply to the optically thick objects. Note that the optically thin objects scatter downwards and to the right, as expected. The solid line is the expected relationship from Dopita & Meatheringham (1990), normalized at $\log (R) = -1.1$ pc.

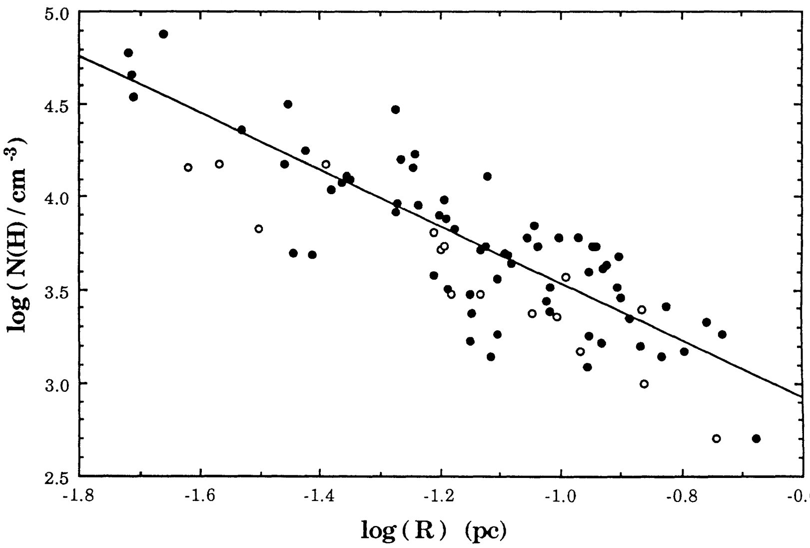

FIG. 7.—Density:diameter relationship inferred for the Magellanic Cloud PN. The symbols have the same meaning as in Figure 5.

Equation (3.4) also implies that there should also be a close correspondence between density and radius, which will also improve if corrections for the luminosity are made. For a constant $\Delta R/R$, n^2/S_* should scale as R^{-3}. For optically thick objects $\Delta R/R$ should increase with R, so the slope of the correlation should be somewhat less steep. In Figure 7 we plot the density: radius relation, and in Figure 8, the $n^2/S_*:R$ relationships, which confirm these expectations.

3.3. *Nebular Abundances*

In Paper I we already gave a complete discussion of the approximations made, and the problems encountered in measuring the abundances through this modeling technique. Since this discussion also applies to this sample, we will not repeat it here, but simply refer the interested reader to Paper I. Table 2 gives the chemical abundances derived for the current sample.

The helium, carbon, and nitrogen abundances are important diagnostics of the various dredge-up processes occurring during the Giant and AGB phase of evolution (Becker & Iben 1980; Renzini & Voli 1981). Although we can say nothing about carbon, the Type I objects stand out as having very large enhancements in nitrogen and helium from the second and third dredge-up episodes. In the second episode, occurring in AGB stars with $M > 3\ M_{\odot}$, both N and He are dredged up. The third phase takes place during the thermal pulsing phase of the AGB, and this increases C/O and He/H at the expense of the N/O ratio. However, the so-called "hot bottom burning" can convert C to N, and so, in principle, produce very large N/O ratios in the PN.

In Figure 9, we plot the N/O ratio as a function of the He/H abundance ratio for the objects modeled in both this paper and in Paper I. Such a diagram has been presented by Henry (1989) to show the distinction between type I and non-type I PN in a

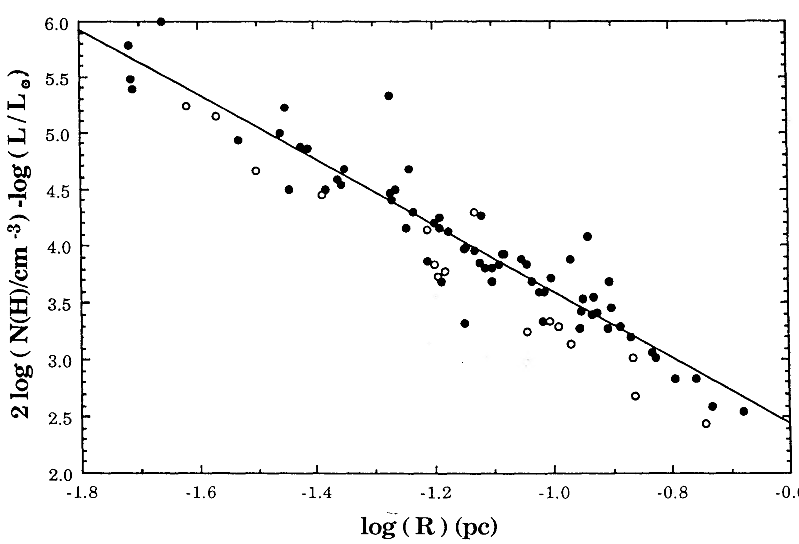

FIG. 8.—"Reduced," i.e., luminosity-corrected density:radius relationship for the Magellanic Cloud PN. The symbols have the same meaning as in Figure 5.

TABLE 2

CHEMICAL ABUNDANCES OF THE PLANETARY NEBULAE DETERMINED FROM NEBULAR MODELS

Object	Chemical Abundances (by Number with Respect to Hydrogen)					
	He	N	O	Ne	S	Ar
LMC						
SMP 02	0.128	1.4E−5	2.3E−4	...	1.6E−6	...
SMP 03	0.085	1.0E−5	1.4E−4	2.0E−5	...	3.0E−7
SMP 06	0.096	2.5E−5	2.2E−4	4.5E−5	6.5E−6	1.5E−6
SMP 07	0.120	1.3E−4	2.2E−4	5.0E−5	2.5E−6	1.6E−6
SMP 13	0.120	9.6E−6	2.0E−4	3.8E−5	3.9E−6	1.6E−6
SMP 14	0.150	1.4E−4	2.0E−4	7.8E−5	4.7E−6	2.7E−6
SMP 16	0.142	1.5E−4	2.3E−4	7.0E−5	7.0E−6	2.5E−6
SMP 19	0.110	3.5E−5	2.8E−4	6.2E−5	9.2E−6	2.4E−6
SMP 24	0.145	2.2E−5	2.4E−4	6.3E−5	2.5E−6	2.2E−6
SMP 29	0.160	1.4E−4	1.8E−4	4.0E−5	8.3E−6	4.5E−6
SMP 32	0.126	1.3E−5	2.0E−4	3.2E−5	2.9E−6	1.5E−6
SMP 33	0.115	4.4E−5	2.6E−4	4.7E−5	9.5E−6	2.1E−6
SMP 35	0.105	2.1E−5	3.0E−4	4.0E−5	2.8E−6	1.8E−6
SMP 38	0.140	4.3E−5	2.0E−4	4.1E−5	1.0E−5	...
SMP 40	0.105	3.9E−5	2.0E−4	6.0E−5	4.6E−6	...
SMP 41	0.110	3.4E−5	2.0E−4	4.2E−5	3.0E−6	2.3E−6
SMP 42	...	8.0E−5	1.7E−4	2.1E−5	3.0E−6	2.0E−6
SMP 44	0.166	1.3E−4	1.8E−4	5.5E−5	3.0E−6	1.5E−6
SMP 45	0.100	2.7E−5	1.8E−4	4.2E−5	7.0E−6	3.0E−6
SMP 46	0.095	6.0E−5	2.0E−4	4.0E−5	1.1E−5	2.4E−6
SMP 48	0.149	2.2E−5	1.7E−4	2.2E−5	...	1.8E−6
SMP 54	0.175	1.8E−4	1.7E−4	7.0E−5	1.0E−5	3.5E−6
SMP 55	0.140	2.5E−5	2.0E−4	3.3E−5	8.0E−6	1.7E−7
SMP 60	0.100	2.5E−5	2.1E−4	2.5E−5	...	...
SMP 61	0.136	1.7E−5	2.2E−4	3.9E−5	7.0E−6	1.6E−6
SMP 62	0.140	2.3E−5	1.7E−4	3.3E−5	8.0E−6	1.1E−6
SMP 67	0.157	1.1E−4	2.4E−4	6.3E−5	5.0E−6	1.7E−6
SMP 72	0.080	1.9E−5	1.4E−4	2.1E−5	...	2.7E−6
SMP 73	0.122	3.2E−5	2.6E−4	5.8E−5	4.9E−6	2.0E−6
SMP 74	0.135	8.0E−6	1.1E−4	1.2E−5	4.0E−6	1.3E−6
SMP 76	0.075	1.2E−5	1.8E−4	2.4E−5	4.0E−6	1.0E−6
SMP 78	0.135	2.8E−5	2.5E−4	4.5E−5	5.2E−6	1.2E−6
SMP 85	0.140	2.8E−5	2.2E−4	3.0E−5	4.0E−6	1.5E−6
SMP 87	0.178	3.1E−4	1.9E−4	1.1E−4	6.8E−6	3.1E−6
SMP 92	0.114	3.5E−5	2.7E−4	5.5E−5	6.6E−6	1.5E−6
SMP 99	0.117	6.5E−5	2.6E−4	3.6E−5	7.3E−6	2.3E−6
SMP 101	0.110	1.7E−5	2.0E−4	4.0E−5	6.0E−6	2.0E−6
SMC						
SMP 02	0.130	7.0E−6	9.0E−5	2.2E−5	1.8E−6	9.0E−7
SMP 03	0.160	...	1.2E−4	1.4E−5	...	7.0E−7
SMP 05	0.130	1.6E−5	1.5E−4	2.5E−5	4.5E−6	1.0E−6
SMP 06	0.135	3.7E−5	1.5E−4	2.2E−5	6.0E−6	8.0E−7
SMP 11	0.090	5.2E−6	1.2E−4	1.5E−5	2.8E−6	1.2E−6
SMP 14	0.100	5.5E−6	1.2E−4	1.3E−5	1.9E−6	1.2E−6
SMP 28	0.190	5.1E−5	5.2E−5	3.0E−5	4.0E−6	1.8E−6

number of galaxies, and has been extensively used by Kaler (1983, 1985) as a diagnostic of the importance of the various dredge-up processes occurring during the giant and AGB phase of evolution. The type I objects stand out as lying on a distinct sequence, indicated on the figure. The N/O ratio is enhanced by a factor of 4 over the other PN, on average, and the sequence displays very little scatter. We know from *IUE* spectra (Aller et al. 1987) that type I objects have low C/O ratios, so therefore some C to N conversion must have occurred in these objects. Since the type I objects have been shown to have more massive core masses, and hence more massive precursors, we can conclude that the C to N conversion is mass-dependent.

Figure 9 also shows that many PN which are not of type I also display moderate enhancements of both N and He over the mean values found in the interstellar medium of the Magellanic Clouds by Russell & Dopita (1990). The N/O ratio can be enhanced by as much as a factor of 4, and the He/H ratio may be as high as 0.15. Together the two sequences of Figure 9 place important new observational constraints upon theoretical dredge-up scenarios.

A further constraint on the dredge-up processes is given by the comparison of N/H with the O/H abundance ratio in the LMC (Fig. 10). Smith & Lambert (1990) have measured these ratios for a number of Galactic red giants which are either O-rich or C-rich. They find a dichotomy, in that the C-rich giants are very much less abundant in N, whereas the O-rich giants show large overabundances of N, and can therefore be expected to evolve to type I PN. The distribution of the type I and non-type I PN in the LMC mirrors this dichotomy

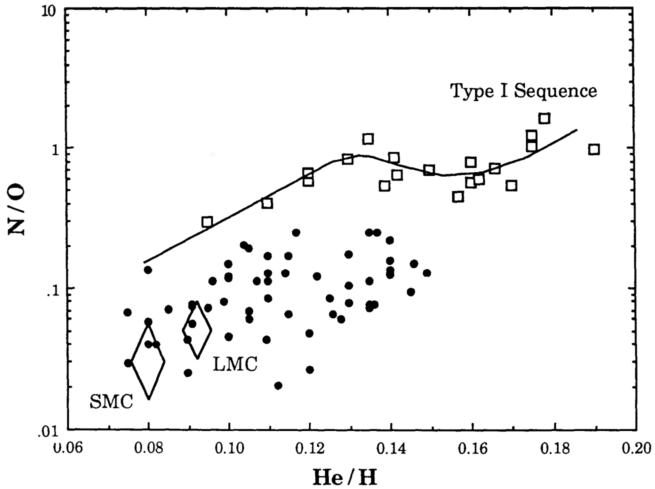

FIG. 9.—Variation of N/O with He/H for nebulae in both the SMC and the LMC. The error diamonds represent the mean abundance ratios for the SMC and the LMC derived from observation of H II regions and SNR by Russell & Dopita (1990). The type I objects are (somewhat arbitarily) defined as those objects having N/O > 0.3. However, it is clear that, even without this distinction, there are quite evidently two separate sequences on this figure.

exactly. What we cannot say until more extensive UV data is available is whether the type I PN are also C-poor. However, it seems likely that this is the case, since the few type I objects which have so far been measured appear to show this property (Aller et al. 1987).

Our abundance data also shows clear evidence for an intrinsic scatter in the abundances of the material which went to form the precursor stars. In Figures 11 and 12 we plot the metallicity-metallicity relationships for those elements which we believe have a simple α-process nucleogenic origin, namely, O, Ne, S, and Ar. In these plots, neon has been selected as the reference element. Oxygen is a primary coolant, is seen in three of its major ionization stages, and both [O II] and [O III] lines are used as primary plasma diagnostics. Argon is seen in three major ionization stages, but suffers from the ionization balance problem discussed in Paper I. Silicon is seen only in two ionization stages [S II] and [S III]. However, the strength of the [S II] lines is strongly dependent on the ionization parameter, and the strength of the 6312 Å [S III] line is strongly dependent

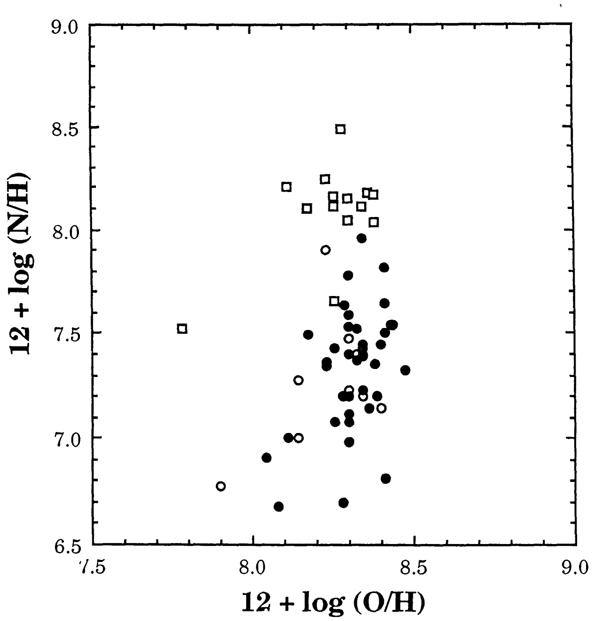

FIG. 10.—N/O ratio as a function of the O/H ratio, plotted in the same way as Smith & Lambert (1990). Note the separation of the type I and non-type I objects on this plot, analogous to the separation which occurs for O-rich and C-rich red giants in the Galaxy.

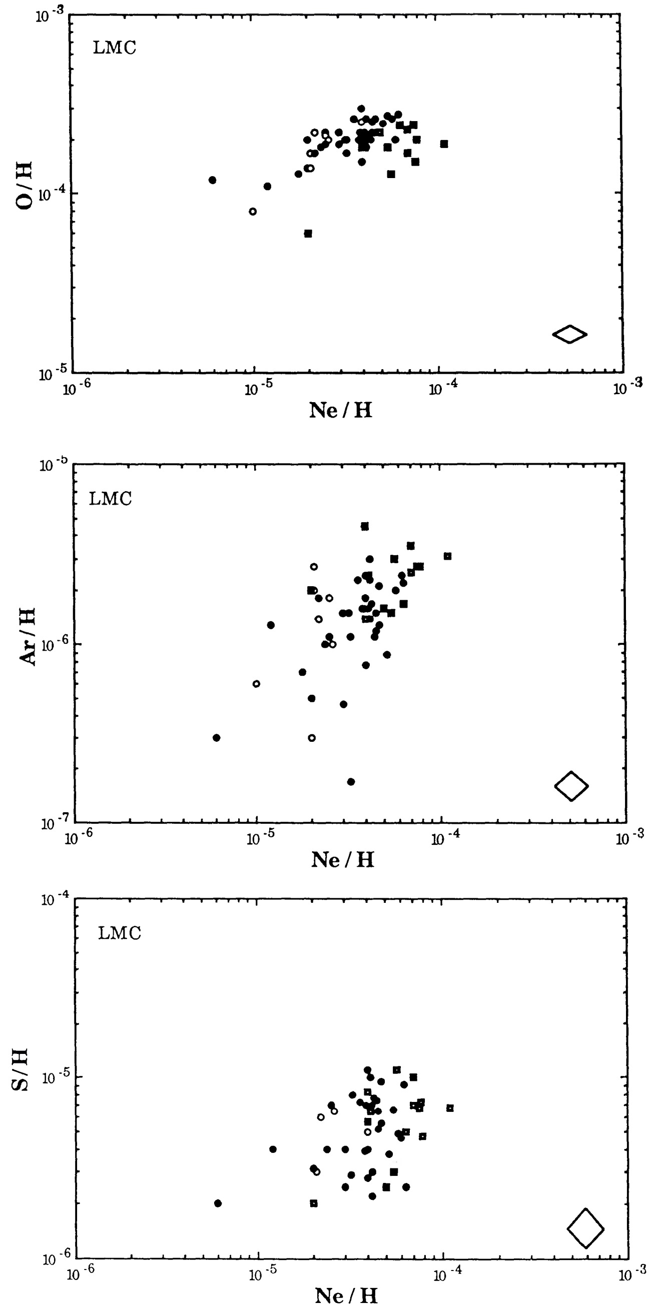

FIG. 11.—Metallicity:metallicity relationships for the LMC PN. Squares represent type I nebulae, closed circles represent optically thick nebulae, and open circles represent optically thin nebulae. A typical error diamond is shown in the lower left-hand corner. Each of these elements should be an Alpha-process element, and therefore any scatter in abundance is intrinsic to the interstellar medium out of which the central star of the PN formed. Note the apparent depletion of oxygen, discussed in the text.

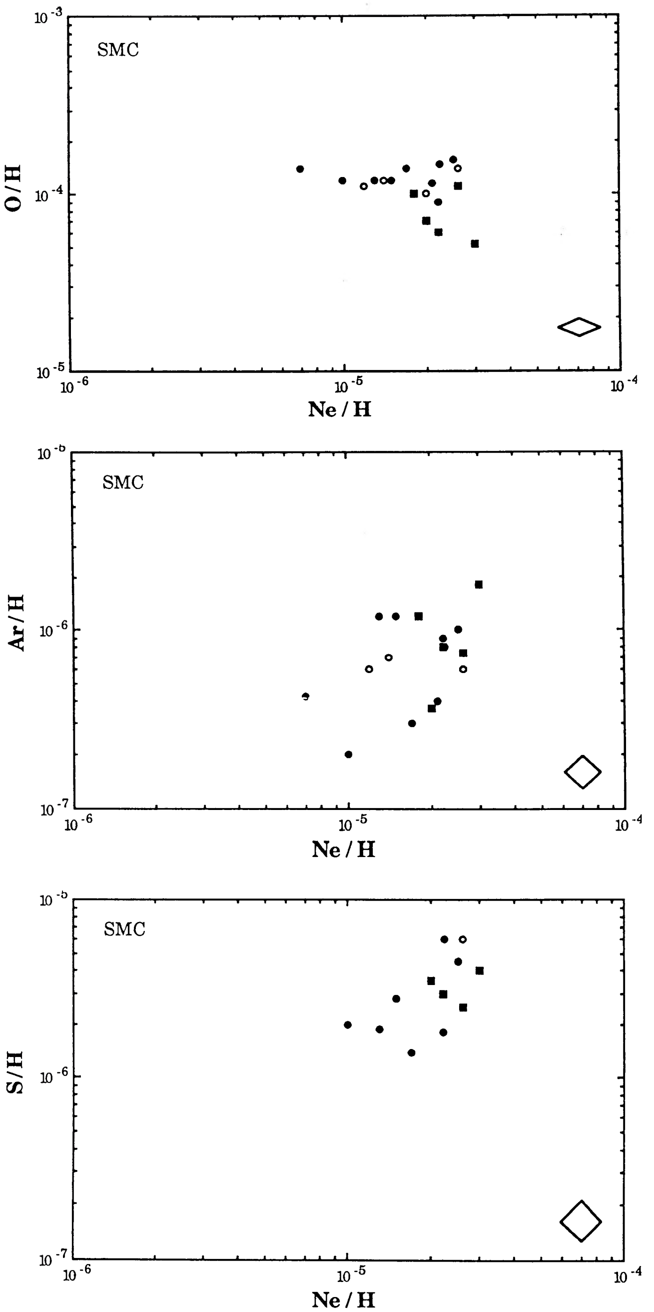

FIG. 12.—Same as Fig. 8, but for the SMC PN. Note that oxygen decreases in abundance even more sharply than the LMC with increasing neon abundance.

on the electron temperature in the zone in which it is produced. For these reasons, the observational error in the abundance determination increases in the sense O to Ar to S.

Any intrinsic abundance scatter over and above the observational error is expected to reveal itself as a spreading of the points along a line of slope unity in these diagrams. It is evident that such a result is true in the case of Ne, Ar, and S. The differences in the current state of chemical evolution of the two clouds are obvious, as the SMC shows lower abundances than the LMC. Also the range of abundance is different. For the LMC, the abundance range is roughly a factor of 10, whilst for the SMC it is smaller, only a factor of 3 to 4. This abundance range presumably encompasses that which existed in the interstellar medium at the time of formation of the PN precursor stars. This supposition is confirmed by the fact that the type I PN, with their massive cores, and presumed youth, are bunched near the upper boundaries of these plots.

What is a surprise in Figures 11 and 12 is the behavior of O. For the LMC, the O abundance reaches a definite maximum, before decreasing with increasing Ne abundance, notably for the type I nebulae. The effect is even more marked in the SMC, where the O abundance appears to show a monatonic decrease with increasing Ne abundance. This result is in distinction to the results of Henry (1989), who derived O and Ne abundances for many PN using published data. His technique relied upon a measurement of the [O III] temperature, and utilised a standard ionization correction factor (ICF) analysis involving O II, O III and Ne III. Henry (1989) found that the O/Ne ratio remains constant over all galaxies for which he had data, and no galaxy showed this roll-off in the O abundance. However, we believe that the result we have obtained is not dependent upon the method of analysis, but is intrinsic to our sample, since, for the LMC, the decrease in the O/Ne ratio at high Ne abundance still shows when the observed [O III]/Hβ ratios are plotted against the observed [Ne III]/Hβ ratio. We suspect that the relatively subtle effect we have found is simply a consequence of improved signal to noise in our data. Any errors in determining the electron temperature would have tended to mask this result by smearing the points along a line of slope unity when Henry's (1989) analysis is employed.

This result is intrinsic to the PN, not to the ISM in general. We agree with Henry's (1989) result that, globally, from galaxy to galaxy, the O/Ne ratio is remarkably constant (e.g., Russell & Dopita 1990). We must therefore look to a physical process unique to PN. One intriguing possibility is that we have found observational evidence for dredge up of ON processed material in the type I PN, which is more severe for PN with lower initial abundances. This is to be expected, since the number of seed nuclei is fewer, and the balance of the CNO nuclei in the H-burning layers will therefore shift from CN cycling equilibrium towards ON equilibrium. If dredge-up and ejection of this material can occur, then this could explain both the decrease on the O abundance, and the very large values of the N/O ratio reached in type I PN (up to 1.6). However, the total amount of material required to be dredged-up required would have to be quite large, in order to produce a net decrease in the oxygen abundance in the nebula by a factor of 2 to 3. It is not clear whether this is allowed by theory.

3.4. *Metallicity-Core Mass Relationships*

The results of the previous subsections have shown that the type I PN are characterized by high metallicity and by larger core masses, and are probably the youngest population of PN in the Clouds. This suggests that core mass may be related with age, and that any chemical evolution of the Clouds with time may show as a core-mass:metallicity relation, provided that the population of PN is old enough. Since the lighter elements we observe are affected to various degrees by dredge-up processes, we restrict our interest here to the heavier α-process elements whose abundances may be reliably determined, Ne and Ar. In Figure 13, we plot the mean α-process abundance with respect to the sun, ([Ne/H] + [Ar/H])/2, as a function of core mass derived from the position of the PN on the H-R diagram with respect to the theoretical tracks. The function of

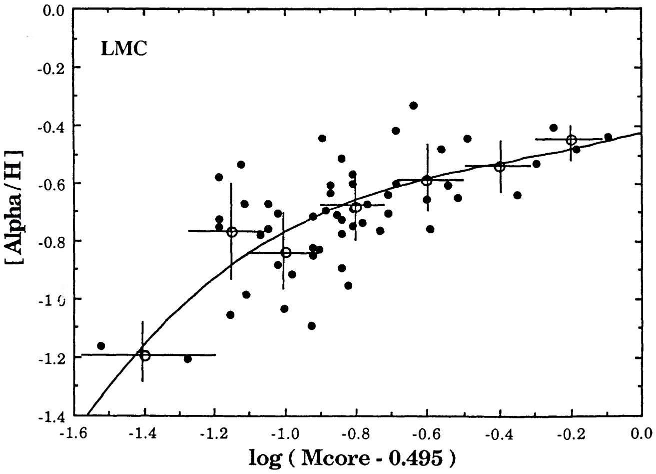

FIG. 13.—Core mass:alpha-process metallicity relationship for the LMC. The "metallicity" is taken as ([Ne] + [Ar])/2.0. This diagram implies that, given a core-mass:age calibration, PN may be used in future to investigate age:metallicity relationships.

core mass, $\log (M_c/M_\odot - 0.495)$ is designed to improve the linearity of the x-axis. This axis is almost linear in the log of the luminosity of the star during its excursion to higher temperatures across the H-R diagram, since Wood & Zarro (1981) showed that these are related through the formula

$$\log (L/L_\odot) = 4.773 + \log (M_c/M_\odot - 0.495) .$$

The correlation of Figure 13 is good, considering the uncertainties of placing individual PN on evolutionary tracks, particularly in the case of PN in the fading portions of the tracks. It would therefore appear that we have discovered a new means to probe the chemical evolution of the Clouds, which will complement the cluster age:metallicity relations (da Costa 1990).

The main problem outstanding before this can be applied directly to the derivation of the age:metallicity relation is to discover a means of calibrating the relationship between core mass and age, or rather, between luminosity at the tip of the AGB and age. Vassiliadis & Wood (1991, in preparation) are in the process of generating self-consistent models for the complete evolution of stars from the main sequence, through to the PN phase. From their very preliminary results, we can estimate that $\log (M_c/M_\odot - 0.495) = -1.4$ corresponds to an age of 15 Gyr, and that $\log (M_c/M_\odot - 0.495) = -0.8$ is of order 2 Gyr. The most massive PN are very young, with ages $< 5 \times 10^8$ yr. It would appear that this technique can, in principle, span the full range of ages needed for the derivation of an age:metallicity relation for the Clouds.

4. CONCLUSIONS

The self-consistent photoionization modeling of a second sample of 44 Magellanic Cloud Planetary Nebulae (PN) has allowed us to construct a Hertzsprung-Russell (H-R) diagram for the central stars in both Clouds, and has given both the nebular chemical abundances and the physical parameters of the nebulae.

The type I PN, are the youngest PN in the Clouds, have the highest core masses, and lie on the descending branch of the evolutionary tracks. These objects show correlated He and N/O abundance enhancements. Part of the N/O enhancement may be the result of ON-processing, since the most extreme type I objects show a depletion of O relative to the other α-process elements such as Ne, S, and Ar.

The nebular mass of the optically thick objects is well-correlated with the nebular radius. However, when we plot the "reduced nebular mass," the ionized mass per unit luminosity as a function of radius, the correlation is much improved. Similarly, density is correlated with radius, but this correlation improves when the effects of luminosity of the central star are corrected for.

We find clear evidence for an abundance scatter in the material which formed the precursor stars of the PN in both the LMC and the MC. This shows clearly in the metallicity-metallicity diagrams for the individual α-process elements, Ne, S, and Ar. The metallicity range in the LMC is a factor of about 10, and is about 3 to 4 for the SMC.

In the case of the LMC, we have also discovered a core-mass:metallicity relation. This is interpreted as a transformed age:metallicity relationship for the LMC. Provided that we can generate a theoretical core mass:age relationship, this offers an interesting observational alternative to the field star and cluster age:metallicity relationships which have been derived for the Magellanic Clouds.

We would like to thank the Anglo-Australian Observatory for the use of their computing facilities. Almost all of the models described in this paper and in Paper I were run on their Vax 3800 at Siding Spring.

REFERENCES

Aller, L. H., Keyes, C. D., Maran, S. P., Gull, T. R., Michalitsianos, A. G., & Stecher, T. P. 1987, ApJ, 320, 159
Barlow, M. J. 1987, MNRAS, 227, 161
———. 1989, in IAU Symposium 131, Planetary Nebulae, ed. S. Torres-Peimbert (Dordrecht: Kluwer), p. 319
Becker, S. A., & Iben, I., Jr. 1980, ApJ, 237, 111
Binette, L., Dopita, M. A., & Tuohy, I. R. 1985, ApJ, 297, 476
da Costa, G. 1990, in IAU Symposium 148, The Magellanic Clouds and Their Dynamical Interaction with the Milky Way, ed. R. Haynes & D. K. Milne (Dordrecht: Kluwer), in press
Dopita, M. A., Ford, H. C., Lawrence, C. J., & Webster, B. L. 1985, ApJ, 296, 390
Dopita, M. A., Ford, H. C., & Webster, B. L. 1985, ApJ, 297, 593
Dopita, M. A., & Meatheringham, S. J. 1990, ApJ, 357, 140
———. 1991, ApJ, 367, 115 (Paper I)
Dopita, M. A., Meatheringham, S. J., Webster, B. L., & Ford, H. C. 1988, ApJ, 327, 639
Dopita, M. A., Meatheringham, S. J., Wood, P. R., Webster, B. L., Morgan, D. H., & Ford, H. C. 1987, ApJ, 315, L107
Feast, M. W., & Walker, A. R. 1987, ARA&A, 25, 345
Gathier, R., Pottasch, S. R., Goss, W. M., & van Gorkom, J. M. 1983, A&A, 128, 325
Henry, R. B. C. 1989, MNRAS, 241, 453
Henry, R. B. C., Liebert, J., & Boroson, T. A. 1989, ApJ, 339, 872
Kaler, J. B. 1983, in Planetary Nebulae, ed. D. R. Flower (Dordrecht: Reidel), p. 245
———. 1985, ARA&A, 23, 89
Meaburn, J., & Walsh, J. R. 1980, MNRAS, 193, 631
Meatheringham, S. J., & Dopita, M. A. 1991a, ApJS, 75, 407
———. 1991b, ApJS, in press
Meatheringham, S. J., Dopita, M. A., Ford, H. C., & Webster, B. L. 1988, ApJ, 327, 651
Meatheringham, S. J., Dopita, M. A., & Morgan, D. H. 1988, ApJ, 329, 166
Meatheringham, S. J., Maran, S. P., Gull, T. R., Stecher, T. P., Michalitsianos, A. G., Aller, L. H., & Keyes, C. D. 1990, ApJ, 361, 101
Middlemass, D., Clegg, R. E. S., Walsh, J. R., & Harrington, J. P. 1991, MNRAS, in press
Monk, D. J., Barlow, M. J., & Clegg, R. E. S. 1988, MNRAS, 234, 583
Morgan, D. H. 1991, in preparation
Morgan, D. H., & Good, A. R. 1985, MNRAS, 213, 491

Pottasch, S. R., & Acker, A. 1989, A&A, 221, 123
Renzini, A., & Voli, M. 1981, A&A, 94, 175
Sanduleak, N., MacConnell, D. J., & Philip, A. G. D. 1978, PASP, 90, 621
Schönberner, D. 1981, A&A, 103, 119
Shaw, R. A. 1989, in IAU Symposium 131, Planetary Nebulae, ed. S. Torres-Peimbert (Dordrecht: Kluwer), p. 473
Smith, V., & Lambert, D. L. 1990, ApJS, 72, 387
Renzini, A., & Voli, M. 1981, A&A, 94, 175
Russell, D. S., & Dopita, M. A. 1990, ApJS, 74, 93
Wood, P. R., Bessell, M. S., & Dopita, M. A. 1986, ApJ, 311, 632
Wood, P. R., & Faulkner, D. J. 1986, ApJ, 307, 659
Wood, P. R., Meatheringham, S. J., Dopita, M. A., & Morgan, D. H. 1987, ApJ, 320, 178
Wood, P. R., & Zarro, D. M. 1981, ApJ, 247, 247
Vassiliadis, E., Dopita, M. A., Morgan, D. H., & Wood, P. R. 1991, ApJ, submitted